Excess nonspecific Coulomb ion adsorption at the metal electrode/electrolyte solution interface: Role of the surface layer

A. M. Gabovich, Yu. A. Reznikov, and A. I. Voitenko*
Institute of Physics, National Academy of Sciences of Ukraine, 46 Nauka Ave., Kyiv 03028, Ukraine
(Received 5 October 2005; revised manuscript received 5 January 2006; published 27 February 2006)

Excess ion adsorption Γ induced by the polarization image forces in the system of a metal electrode/symmetric electrolyte solution separated by an insulating interlayer has been calculated. The adopted theoretical scheme involves the Coulomb Green's function in a three-layer system with sharp interfaces and specular reflection at them. The influence of the spatial dispersion of the dielectric permittivities $\varepsilon_i(\mathbf{k})$ in all the three media on the image force energy W_{im} and the adsorption Γ has been analyzed, where $\mathbf{k}$ is the wave vector. A comparison with the classical model, where ε_i=const, has been carried out. It has been shown that both the Debye-Hückel ion screening and the spatial dispersion of the solvent contribution $\varepsilon_{\mathrm{solv}}(\mathbf{k})$ to the overall dielectric function $\varepsilon_{\mathrm{el}}(\mathbf{k})$ of the electrolyte solution lead to the qualitative difference with the results for the classical model. In particular, in a wide range of ion concentrations n_0 a thin interlayer $L \geqslant 5-10$ Å effectively screens out the attractive influence of the metallic electrode, so that the net Coulomb adsorption may become repulsive. The approach and the results obtained qualitatively describe two physically different situations. Specifically, the introduced interlayer corresponds either to the dense near-electrode (inner) electrolyte layer or to the intentionally deposited control coating of arbitrary thickness.

DOI: 10.1103/PhysRevE.73.021606 PACS number(s): 68.03.−g, 77.22.Ch, 82.45.Un, 68.43.−h

I. INTRODUCTION

The influence of image-force energies at the interfaces between two plasmalike media, such as metals and electrolyte solutions, has been the subject of widespread investigations for rather a long period [1], although the role of polarization phenomena is sometimes underestimated [2]. One should keep in mind that even the well-known simplest, quoted in textbooks, classical expression for this kind of electrostatic energy, which describes the case of constant dielectric permittivities ε_i's on either side of the common interface, hides its complicated quantum-mechanical background [3,4]. When the spatial dispersion of the dielectric permittivities $\varepsilon(\mathbf{k})$'s is accounted for, a further level of complexity arises [5,6]. Here $\mathbf{k}$ is the wave vector. The variety of model $\varepsilon(\mathbf{k})$ dependences for solvents as hosts for embedded ions describe rich physics and chemistry both in the bulk of electrolyte solutions [7–18] and near their interfaces [19–25] with other plasmalike media.

All this diversity goes back to the Inkson basic interpolation formula

$$\varepsilon_I(\mathbf{k}) = \varepsilon_* + \frac{\varepsilon_0 - \varepsilon_*}{1 + \dfrac{\varepsilon_0}{\varepsilon_*}\Lambda^2 k^2}, \tag{1}$$

which was first developed for semiconductors [26] and takes into account the peculiarities of a test charge $\tilde{e}$ screening by their bound electrons. Here, ε_0 is the macroscopic (long-wavelength) static dielectric constant, ε_* the short-wavelength one, and Λ the correlation length of bound electrons. In the solvent, the constitutive entities are solvent molecules, but the character of screening is very similar to that by valence electrons in semiconductors. The parameter Λ has now the meaning of the solvent intermolecular correlation length.

At the same time, the dissolved ions give rise to the Debye-Hückel contribution

$$\varepsilon_{DH}(\mathbf{k}) = \frac{\varepsilon_0 \kappa^2}{k^2}, \tag{2}$$

where κ is the relevant inverse screening radius, so that the overall dielectric function becomes

$$\varepsilon(\mathbf{k}) = \varepsilon_I(\mathbf{k}) + \varepsilon_{DH}(\mathbf{k}). \tag{3}$$

Hereafter, for simplicity, we consider only a 1:1 electrolyte solution, so that κ equals $(8\pi n_0 e^2/k_B T\varepsilon_0)^{1/2}$, n_0 is the bulk concentration of each kind of ions, e the elementary charge, T the absolute temperature, and k_B the Boltzmann constant.

The dielectric mismatch at the boundary between a metallic (or semiconducting) electrode and an electrolyte solution may result in the nonmonotonic spatial profile of the image-force energy W_{im} in the solution both when the latter is treated as a plasmalike Debye-Hückel medium [5,27,28] or described by Eq. (3) [20,29]. Moreover, such a behavior of the image forces leads to the nonmonotonic *concentration* dependence of the excess electrostatic nonspecific adsorption $\Gamma(n_0)$ and the corresponding excess surface tension $\Delta\sigma(n_0)$ at the point of zero charge [20,27–31]. At the vacuum/electrolyte solution interface, on the contrary, the respective concentration dependences $\Gamma(n_0)$ and $\Delta\sigma(n_0)$ are monotonic [32].

The results cited above were obtained using the abrupt interface model and assuming the specular quasiparticle reflection at the medium interfaces [33–35]. In actual truth, however, the metal electrons spill out over the positive back-

*Electronic address: collphen@iop.kiev.ua

ground edge into the electrolyte solution, making the dielectric characteristics highly inhomogeneous [36], so that the important problem of the electrochemical contact capacity requires more involved approaches [37]. At the same time, while calculating such integral properties as the electrostatic excess adsorption, the degree of the interface diffusivity becomes less important (see a comparison between different kinds of the dielectric approximations [38]).

On the other hand, according to the totality of experimental data and dominating theoretical ideas, the electrolyte solution can be divided into a dense near-electrode (inner) electrolyte layer and a diffusive (outer) one evolving into the bulk of the solution [36,39]. To make allowance for the dense near-electrode shell, it is necessary to consider a three-layer rather than a two-layer system, with different dielectric characteristics inherent to each medium involved. An interlayer theoretically introduced in that way may also describe a thin insulating coating, intentionally deposited on the metal to control the physical adsorption. Then, notwithstanding the high polarizability of a metal, one could even change the adsorption sign.

Thus, in this paper we calculated the image-force energy W_{im} and the electrostatic contribution to the nonspecific ion adsorption $\Gamma(n_0)$ in a three-layer electrochemical system. The spatial dispersion of the medium dielectric permittivities was accounted for. In doing so, we used the general approach elaborated earlier [34,40,41].

Knowing the profile of the image-force energy in three-layer structures is important, because it is the input quantity in solving many electrochemical, biological, and solid-state issues. First of all, we mean standard electrochemical cells: metallic electrode–dense layer–outer layer, although the crossover between last two media is gradual [36,39]. In other systems, both interfaces are well defined. In particular, our theory is applicable to semiconductor heterostructures [42–45], to metal-oxide-semiconductor structures [46–49], to lamellar systems, where an electrolyte solution is confined between dielectric covers (lipid membranes, in particular) [22,24,50–56], or to a liquid crystal (LC) lipid membrane surrounded by two electrolyte solutions [57,58].

One can indicate another very important area of application of the three-layer image-force theory developed here. We have in view electro-optics and nonlinear-optics LC devices (LCDs), e.g., optical switchers and photorefraction devices [59]. The matter is that LCs, as other organic liquids, are weak electrolytes and contain ions which interact electrostatically with the polymer aligning layers covering metallic electrodes in LC cells. The amorphous tungsten trioxide WO_3 may also be a building material for asymmetric nematic LC cells [60,61]. As a consequence of the electrostatic interaction, a nonspecific physical adsorption of charged particles arises [20,27–32,62–70], which leads to the formation of a charged surface layer partially compensating the applied electric field in the bulk of the LC. The energy W_{im} makes the main contribution $\Gamma(n_0)$ to this kind of adsorption and hence governs transport processes in LC cells and operational properties of the latter.

It should be noted that the very choice of the Inkson-like description $\varepsilon_I(k)$ of the solvent screening ability is not crucial. Actually, the interpolation character of $\varepsilon_I(k)$ reflects only its being a bridge between the proper long-wavelength and short-wavelength limits. The true dielectric function of the solvent may be quite different, although these asymptotic limits should be retained in any case. For instance, in the case of solid semiconductors, Schulze and Unger [71] modified $\varepsilon_I(k)$ in such a way that their modification $\varepsilon_{SU}(\mathbf{k})$ differs from the former for large $\mathbf{k}$. Namely, $\varepsilon_{SU}(\mathbf{k})$ falls off as $\sim k^{-4}$ at large $\mathbf{k}$. Such a choice is a consequence of the following quantum-mechanical arguments. Since the response of any valence electron to a test charge at extremely small distances between them does not depend on existing molecular bonds, screening of the test charge by bound electrons should coincide with that by the free electron gas. On the other hand, the screening by free electrons should reflect the quantum nature of the degenerate electrons in the limit of large $\mathbf{k}$ [72,73], where the semiclassical Thomas-Fermi description fails. Hence, the advantages of $\varepsilon_{SU}(\mathbf{k})$ over the basic $\varepsilon_I(\mathbf{k})$ are the same as the superiority of the Lindhard dielectric function over its Thomas-Fermi counterpart.

It is remarkable that the usage of $\varepsilon_{SU}(\mathbf{k})$ instead of $\varepsilon_I(\mathbf{k})$ improves the behavior of image forces near the semiconductor-vacuum interface, so that not only the image-force energy but also the force itself do not diverge [74,75]. Nevertheless, the deviations are conspicuous only within a thin layer $\lesssim\Lambda$, whereas the adsorption Γ, which is the quantity of interest here, constitutes an integral over all distances [see Eq. (14)]. Therefore, it is not essentially altered by the quantum-mechanical correction to the image forces, although the latter is very important *per se*. It means that the qualitative features of $\Gamma(n_0)$ found below including its nonmonotonic character would survive the replacement of $\varepsilon_I(\mathbf{k})$ by $\varepsilon_{SU}(\mathbf{k})$ or any other approximation formula of that kind.

The discussion so far concerned only a class of solvent dielectric functions monotonic in $\mathbf{k}$-space. At the same time, some speculations exist, according to which more complex forms of $\varepsilon(\mathbf{k})$ may occur including $\mathbf{k}$ intervals with $\varepsilon(\mathbf{k})<0$ [11,12]. This overscreening [14] is a very interesting possibility that arises when local-field effects [76,77] are extremely strong; any general principle is not violated in this case. At the same time, the actual limitations on the proper response function $\varepsilon^{-1}(\mathbf{k},\omega)$ do exist and agree with the Le Chatelier-Braun principle, according to which the response of a stable system to a perturbation reduces the action of the latter [78,79]. Recent calculations [18] show that the corresponding oscillations of the electrostatic potential in the interfacial water might explain the analogous experimental data in certain biological objects [56], hydrophilic cleavage planes of the calcite and barite ionic crystals [55], and the mica(001)-water interface [80]. Such intriguing cases are left beyond the scope of this paper dealing with more conventional and typical situations.

The scheme of the article is as follows. The formulation of the problem is outlined in Sec. II. Section III is devoted to numerical calculations and the relevant discussion. The conclusions are contained in Sec. IV.

II. FORMULATION

We consider a three-layer system, with each constituting medium $(i=1,2,3)$ described by a bulk dielectric function

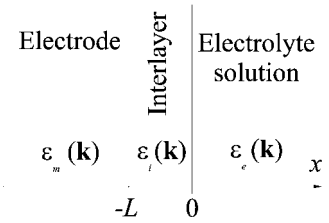

FIG. 1. Three-layer sandwich: electrode–interlayer–electrolyte solution.

$\varepsilon_i(\mathbf{k})$ (see Fig. 1). The semi-infinite covers of the sandwich are the metal electrode and the symmetric 1:1 electrolyte solution, while the interlayer represents either the dense (Helmholtz) layer or a thin-film electrode coating. Hereafter, we also use the sub- or superscripts *m*, int, el, and solv for the metallic electrode, the interlayer, the electrolyte solution, and the solvent background, respectively, where needed. The Coulomb energy of a charge *e* in every medium can be found by the conventional procedure of solving the Poisson equations and matching the solutions at specularly reflecting smooth plane interfaces [34,40,41]. Since the concrete calculations concern only the electrolyte solution ($i=1$), all the expressions below for Coulomb energies correspond to this medium. Therefore, in subsequent formulas the medium-characterizing subscript is indicated only in the cases when it is necessary for clarity.

The total Coulomb energy of an ion with the unitary charge $\pm e$ in the 1:1 solution (medium 1) is given by the formula

$$W_{\mathrm{Coul}}(x) = -e^2 \int_0^\infty qdq \left[D(q;x,x) + \frac{1}{2q\varepsilon_1(k\to\infty)} \right]. \quad (4)$$

Here, $\varepsilon_1(k\to\infty)$ is the short-wave limit of the solution dielectric permittivity, which is, strictly speaking, equal to unity, since screening disappears at short distances. Nevertheless, we shall retain the expression $\varepsilon_1(k\to\infty)$, first, for generality, and, second, because this parameter enters into various model approximation formulas for $\varepsilon(k)$ and thus may deviate from unity. The function $D(q;x,x)=\lim_{x'\to x} D(q;x,x')$, where $D(q;x,x')$ is the Green's function of the self-consistent electromagnetic field [34,40,41,81], and is the functional of the bulk dielectric functions $\varepsilon_i(\mathbf{k})$ of the media involved

$$D(q;x,x) = \frac{a_1^2(q,x)}{B(q)}[a_S(q,0) + a_A(q,0) + 2a_3(q,L)] - b_1(q;x,x), \quad (5)$$

$$a_1(q,x) = \frac{1}{\pi}\int_{-\infty}^{\infty} \frac{dk_\perp e^{ik_\perp x}}{(k_\perp^2+q^2)\varepsilon_1(k_\perp,q)}, \quad (6)$$

$$a_3(q,x) = \frac{1}{\pi}\int_{-\infty}^{\infty} \frac{dk_\perp \exp[ik_\perp(x-L)]}{(k_\perp^2+q^2)\varepsilon_3(k_\perp,q)}, \quad (7)$$

$$a_{S,A}(q,x) = \frac{2}{L}\sum_{k_\perp^{S,A}} \frac{\exp(ik_\perp x)}{(k_\perp^2+q^2)\varepsilon_2(k_\perp,q)}, \quad (8)$$

$$k^2 = q^2 + k_\perp^2,\ k_\perp^S = 2n\frac{\pi}{L},\quad k_\perp^A = (2n+1)\frac{\pi}{L},$$

$$n = 0, \pm 1, \pm 2, \ldots, \quad (9)$$

$$b_1(q;x,x') = \frac{1}{2}[a_1(q,x+x') + a_1(q,x-x')], \quad (10)$$

$$B(q) = [a_S(q,0) + a_1(q,0)][a_A(q,0) + a_3(q,L)] + [a_S(q,0) + a_3(q,L)][a_A(q,0) + a_1(q,0)]. \quad (11)$$

Here, *L* is the thickness of the near-electrode layer. It should be noted that the very existence of blocks (6)–(8) is the consequence of our assumption that quasiparticles are reflected specularly at the interfaces.

It is precisely the quantity $W_{\mathrm{Coul}}(x)$ rather than the related image-force energy $W_{\mathrm{im}}(x)$ (see below) that is continuous across the medium boundaries, if the proper limits $\varepsilon_i(k\to\infty)=1$ take place. [This subtle issue was discussed at length in Refs. [27,28]. On the other hand, in the important paper (Ref. [40])], both energies were confused, although the starting formulas were correct there.) The electrostatic polarization energy $W_{\mathrm{Coul}}(x)$ consists of two terms: $W_{\mathrm{Coul}}(x) = W_{\mathrm{bulk}} + W_{\mathrm{im}}(x)$. The first one, W_{bulk}, is a homogeneous polarization energy of the test charge in the bulk of the solution. It can be easily derived from Eq. (4) by switching off all the effects that are induced by the adjacent media (the electrode and the interlayer),

$$W_{\mathrm{bulk}} = -e^2 \int_0^\infty qdq \left[\lim_{x\to\infty} D(q;x,x) + \frac{1}{2q\varepsilon_1(k\to\infty)} \right]. \quad (12)$$

In essence, it is a difference between the infinite charge self-energy in the medium concerned with all spatial-dispersion effects of the respective dielectric function switched off and the infinite energy of the shielding cloud. The second component, $W_{\mathrm{im}}(x)$, is due to the existence and charge polarization of other media. Naturally, the item depends on the charge position *x* relative to the medium interfaces. This quantity is called the image force energy $W_{\mathrm{im}}(x)$ and can be found by subtracting W_{bulk} from the total Coulomb energy $W_{\mathrm{Coul}}(x)$,

$$W_{\mathrm{im}}(x) \equiv W_{\mathrm{Coul}}(x) - W_{\mathrm{bulk}} = -e^2\int_0^\infty qdq[D(q;x,x) - \lim_{x\to\infty} D(q;x,x)] = -e^2\int_0^\infty qdq\left\{ \frac{a_1^2(q,x)}{B(q)} \times [a_S(q,0) + a_A(q,0) + 2a_3(q,L)] - \frac{1}{2}a_1(q,2x) \right\}. \quad (13)$$

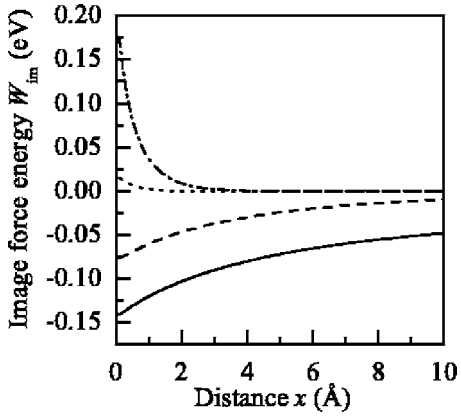

FIG. 2. Image-force energy profiles $W_{\mathrm{im}}(x)$ for a unit charge in the 1:1 Debye-Hückel electrolyte ion (a dispersionless solvent dielectric permittivity, $\varepsilon_0^{\mathrm{solv}}$=const) and various concentrations n_0, separated from a classical metallic electrode ($\varepsilon_m^0=\infty$) by an insulating interlayer ($\varepsilon_0^{\mathrm{int}}$=const). The so-called neutral case $\varepsilon_0^{\mathrm{int}}=\varepsilon_0^{\mathrm{solv}}=5$. The interlayer thickness $L=5$ Å. The ion concentration $n_0=0$ (solid), 10^{18} (dashed), 10^{19} (dotted), and 10^{20} cm^{-3} (dotted-dashed curve).

Even if all the relevant dielectric permittivities satisfy the limit $\varepsilon_i(k\to\infty)=1$, we have $W_{\mathrm{im,el}}(L+0)\neq W_{\mathrm{im,int}}(L-0)$ and $W_{\mathrm{im,int}}(+0)\neq W_{\mathrm{im,m}}(-0)$, because the bulk polarization energies are different for each medium. The quantity $W_{\mathrm{im}}(x)$ derived in this manner is the analog of the image-force energy obtained for the case of only one interface by the Güntelberg charging method [82].

The image forces lead to the enrichment or depletion of the electrolyte surface shell in dissolved ions [20,27–32,83,84]. The corresponding extra electrostatic adsorption for each ion species is given as follows:

$$\Gamma = n_0 \int_0^\infty dx \left[\exp\left(-\frac{W_{\mathrm{im}}(x)}{k_B T} \right) - 1 \right]. \tag{14}$$

The overall electrostatic adsorption is twice as much as that given by Eq. (14). As has already been indicated in the Introduction, the adopted approach is a simplification because it neglects the interface roughness [85,86] and the complex

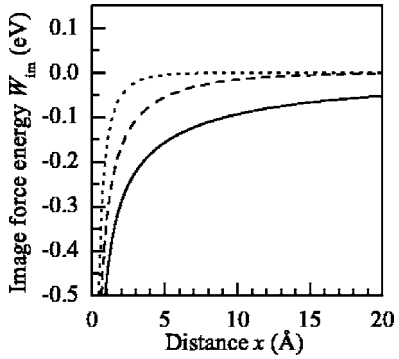

FIG. 3. The same as in Fig. 2 but for the attractive case $\varepsilon_0^{\mathrm{int}}>\varepsilon_0^{\mathrm{solv}}$ ($\varepsilon_0^{\mathrm{int}}=5$, $\varepsilon_0^{\mathrm{solv}}=3$). $L=5$ Å. $n_0=0$ (solid), 10^{18} (dashed), and 10^{19} cm^{-3} (dotted curve).

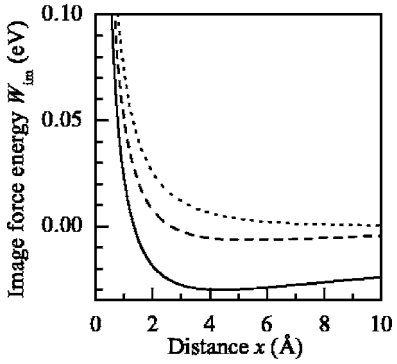

FIG. 4. The same as in Fig. 2 but for the repulsive case $\varepsilon_0^{\mathrm{int}}<\varepsilon_0^{\mathrm{solv}}$ ($\varepsilon_0^{\mathrm{int}}=5$, $\varepsilon_0^{\mathrm{solv}}=8$). $L=5$ Å. $n_0=0$ (solid), 10^{18} (dashed), and 10^{19} cm^{-3} (dotted curve).

structure of the double layer [2,19,25,36,37]. Nevertheless, it gives a useful insight into the problem and allows one to estimate the magnitude of possible effects.

III. CALCULATIONS

A. Dispersionless (classical) dielectric permittivities

It is instructive to consider first the classical case of constant permittivities ε_i in all the three media. Then, substituting Eqs. (6)–(8), into integral (13), one easily obtains the following expression for the image-force energy in medium 1:

$$W_{\mathrm{im}}(x) = -\frac{e^2}{4\varepsilon_1}\frac{\varepsilon_3-\varepsilon_1}{\varepsilon_3+\varepsilon_1}\left\{\frac{1}{x} - I_1(x)\right\}, \tag{15}$$

where

$$I_1(x) = 4\frac{\varepsilon_1}{\varepsilon_2}\frac{\varepsilon_2^2-\varepsilon_3^2}{\varepsilon_1^2-\varepsilon_3^2}\int_0^\infty \frac{dq e^{-2qx}\tanh(qL)}{1+\dfrac{\varepsilon_2}{\varepsilon_3+\varepsilon_1}\left(1+\dfrac{\varepsilon_3\varepsilon_1}{\varepsilon_2^2}\right)\tanh(qL)}. \tag{16}$$

Isolating the x^{-1}-term from integral (16), we arrive at the expression

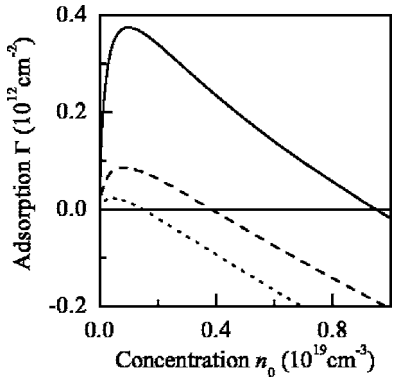

FIG. 5. Dependences of the excess surface adsorption Γ on the 1:1 Debye-Hückel electrolyte solution ion concentration n_0 in the system classical metallic electrode–interlayer with a constant dielectric permittivity–solvent with a constant dielectric permittivity for various $\varepsilon_0^{\mathrm{solv}}\geq\varepsilon_0^{\mathrm{int}}$ (a repulsive interlayer). $L=5$ Å, $\varepsilon_0^{\mathrm{int}}=5$. $\varepsilon_0^{\mathrm{solv}}=5$ (solid), 6 (dashed), and 8 (dotted curve).

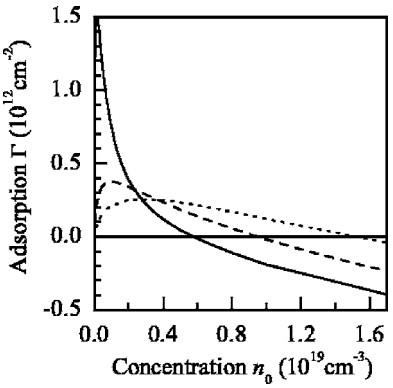

FIG. 6. The same as in Fig. 5 but for the model of ion-free near-electrode interlayer: $\varepsilon_0^{\text{solv}}=\varepsilon_0^{\text{int}}=3$ (solid), 5 (dashed), and 8 (dotted curve). $L=5$ Å.

$$W_{\text{im}}(x) = -\frac{e^2}{4\varepsilon_1 x}\frac{\varepsilon_2-\varepsilon_1}{\varepsilon_2+\varepsilon_1} + I_2(x), \tag{17}$$

where

$$I_2(x) = \frac{e^2(\varepsilon_2-\varepsilon_3)}{(\varepsilon_1+\varepsilon_2)(\varepsilon_3+\varepsilon_1)} \times \int_0^\infty \frac{dqe^{-2qx}[1-\tanh(qL)]}{1+\frac{\varepsilon_2}{\varepsilon_3+\varepsilon_1}\left(1+\frac{\varepsilon_3\varepsilon_1}{\varepsilon_2^2}\right)\tanh(qL)} \tag{18}$$

Integral (18) is finite at any $x \geqslant 0$, so at $x \to 0$ the augend in expression (17) dominates for any values of the parameters ε_i. Thus, without regard to the particular ε_3 (electrode) dielectric constant, the sign of the $W_{\text{im}}(x)$ function near the solution/interlayer boundary and, to some extent, the character of the excess adsorption are determined by the relationship between ε_1 and ε_2. In accordance with this relation, we may classify their possible combinations as attractive ($\varepsilon_1 < \varepsilon_2$), repulsive ($\varepsilon_1 > \varepsilon_2$), and neutral ($\varepsilon_1 = \varepsilon_2$) ones. In the case $\varepsilon_2=\varepsilon_1$, the first term in expression (17) vanishes, and integral (18) is calculated exactly, so that

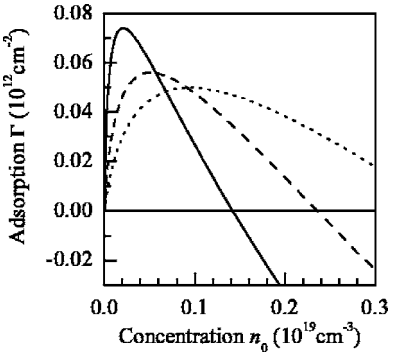

FIG. 7. The same as in Fig. 6 but for $L=10$ Å.

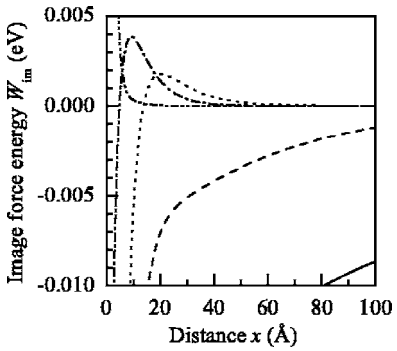

FIG. 8. Image-force energy profiles $W_{\text{im}}(x)$ for a unit charge in the 1:1 Debye-Hückel electrolyte solutions separated from a classical metallic electrode ($\varepsilon_m^0=\infty$) by an insulating interlayer with $L=10$ Å for various ion concentrations $n_0=0$ (solid), 10^{16} (dashed), 10^{17} (dotted), 10^{18} (dotted-dashed), and 10^{19} cm^{-3} (dotted-dotted-dashed curve). The spatial dispersion of dielectric permittivity is taken into account both for the interlayer and the solvent. The parameters are $\varepsilon_0^{\text{int}}=10$, $\varepsilon_0^{\text{solv}}=3$ ($\varepsilon_0^{\text{int}} > \varepsilon_0^{\text{solv}}$), $\Lambda_{\text{int}}=5$ Å, and $\Lambda_{\text{solv}}=7$ Å ($\Lambda_{\text{int}} < \Lambda_{\text{solv}}$). Note the attractive relationship between the dielectric long-wavelength constants $\varepsilon_0^{\text{int}}$ and $\varepsilon_0^{\text{solv}}$.

$$W_{\text{im}}(x \geqslant 0) = -\frac{e^2}{4\varepsilon_1(x+L)}\frac{\varepsilon_3-\varepsilon_1}{\varepsilon_3+\varepsilon_1}, \tag{19}$$

as it has to be, because the interlayer becomes electrostatically indistinguishable from the solution. In the case $\varepsilon_2=\varepsilon_3$, i.e., if the interlayer can be considered as a continuation of the electrode, integral $I_1(x)$ in (15) vanishes, and

$$W_{\text{im}}(x) = -\frac{e^2}{4\varepsilon_1 x}\frac{\varepsilon_3-\varepsilon_1}{\varepsilon_3+\varepsilon_1}. \tag{20}$$

In other words, one may view the electrostatic effect of the three-layer system (Fig. 1) on a charge located in medium 1 in a twofold manner. First, the three-layer system may be regarded as a two-layer one, composed of two semi-infinite covers (media 1 and 3) and modified by the insertion of an interlayer (medium 2) between them. According to this interpretation, $W_{\text{im}}(x)$ can be easily recognized as the classical image-force energy (19) caused by the dielectric mis-

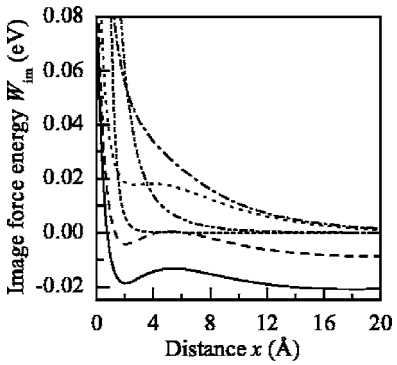

FIG. 9. The same as in Fig. 8 but for $\Lambda_{\text{solv}}=3$ Å and $\Lambda_{\text{int}}=5$ Å ($\Lambda_{\text{solv}} < \Lambda_{\text{int}}$). $n_0=0$ (solid), 10^{16} (dashed), 10^{17} (dotted), 10^{18} (dotted-dashed), 10^{19} (dotted-dotted-dashed curve), and 10^{20} cm^{-3} (short-dashed curve).

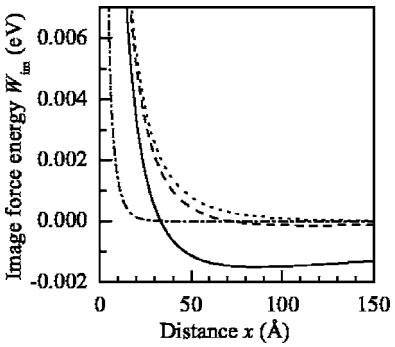

FIG. 10. The same as in Fig. 9 but for $\varepsilon_0^{\text{int}}=3$ and $\varepsilon_0^{\text{solv}}=10$ ($\varepsilon_0^{\text{int}}<\varepsilon_0^{\text{solv}}$). $n_0=0$ (solid), 10^{16} (dashed), 10^{17} (dotted), and 10^{19} cm^{-3} (dotted-dashed curve).

match between cover media 1 and 3 and screened by the induced polarization in slab 2. But since charges in the slab interact not only with their counterparts in cover 1 but also with those in cover 3, the latter modifies the screening ability of the charges in medium 2 as well. It is evident that for $L\to 0$ this modification disappears.

According to the second point of view [Eq. (17)], the system is composed of two formally semi-infinite covers (media 1 and 2), but the dielectric response of medium 2 (interlayer) is modified by the existence of the electrode (medium 3). It is worth noting that the image force energy in three-layer systems with *constant* ε_i's has been examined in different contexts [46–48,87,88]. An explicit analytical expression for $W_{\text{im}}(x)$ in the outermost layer, similar to Eq. (15) (but in another form), has been introduced for the first time, as far as we know, in Ref. [87].

If metal 3 is treated as an ideal conductor ($\varepsilon_3\to\infty$), expression (15) can be simplified further as follows:

$$W_{\text{im}}(x)=-\frac{e^2}{2\varepsilon_1}\int_0^\infty dq e^{-2qx}\frac{1-\dfrac{\varepsilon_1}{\varepsilon_2}\tanh(qL)}{1+\dfrac{\varepsilon_1}{\varepsilon_2}\tanh(qL)}. \qquad (21)$$

Of course, the textbook result $-e^2/(4\varepsilon_1 x)$ stems from Eq. (21) when $L\to 0$.

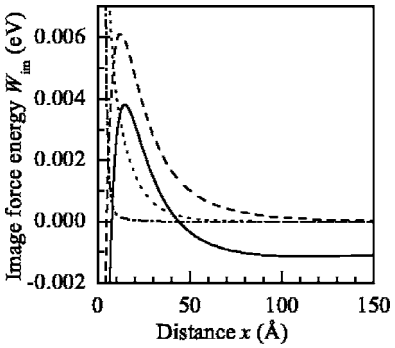

FIG. 11. The same as in Fig. 10 but for $\Lambda_{\text{solv}}=7$ Å and $\Lambda_{\text{int}}=5$ Å ($\Lambda_{\text{solv}}>\Lambda_{\text{int}}$). $n_0=0$ (solid), 10^{17} (dashed), 10^{18} (dotted), and 10^{19} cm^{-3} (dotted-dashed curve).

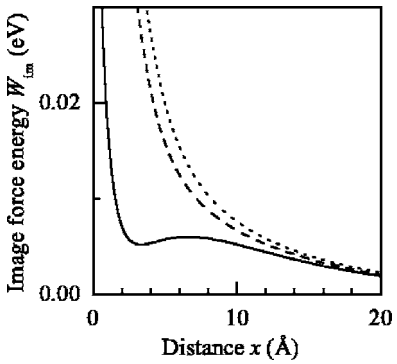

FIG. 12. Image-force energy profiles $W_{\text{im}}(x)$ at $\Lambda_{\text{int}}=\Lambda_{\text{solv}}=5$ Å, $\varepsilon_0^{\text{int}}=3$, $\varepsilon_0^{\text{solv}}=10$ ($\varepsilon_0^{\text{int}}<\varepsilon_0^{\text{solv}}$), and $n_0=10^{18}$ cm^{-3} for various interlayer thicknesses $L=5$ (solid), 10 (dashed), and 100 Å (dotted curve).

The very presence of the interlayer (even when it is a comparatively thin film) shifts the metallic medium away to the position where the distinction between any specific electrode and the ideal conducting half-space becomes negligible. Indeed, roughly speaking, the electron gas spills out over a distance of the order of the Thomas-Fermi length L_{TF} [36,89,90]. Therefore, for typical metallic electrode materials and $L\gtrsim 5$ Å $\gtrsim L_{\text{TF}}$, the inhomogeneous distribution of electrons both inside and outside the electrode will not affect the metal polarization drastically under the influence of an electrolyte's ion charge. It means that medium 3 (the electrode) can be regarded as an ideal conductor with $\varepsilon_0^m=\infty$. Therefore, to avoid cumbersome although insignificant details of the metal screening ability, we shall confine ourselves to this case in the following sections. One should keep in mind, however, that the double-layer structure and the electric capacity *do depend* on the nonhomogeneous character of the metal-solution interface and are determined by all constituents of the three-layer sandwich [37].

B. Dispersionless solvent and interlayer dielectric functions

Taking into account the spatial dispersion of dielectric permittivities of the media prohibits from obtaining most results in the analytical form. Some of them for a two-layer system can be found in other works [20,29–31]. For the

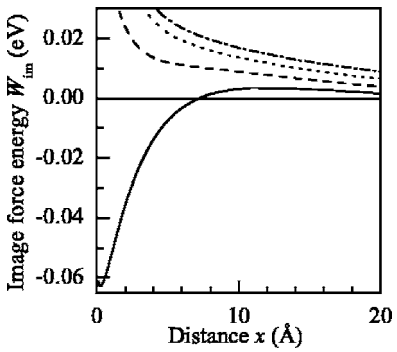

FIG. 13. The same as in Fig. 12 but for $n_0=0$. $L=5$ (solid), 10 (dashed), 30 (dotted), and 100 Å (dotted-dashed curve).

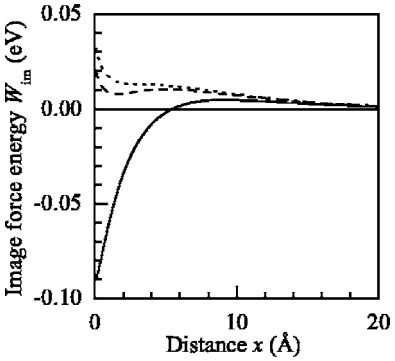

FIG. 14. The same as in Fig. 12 but for $\varepsilon_0^{\text{int}}=10$ and $\varepsilon_0^{\text{solv}}=3$ ($\varepsilon_0^{\text{int}}>\varepsilon_0^{\text{solv}}$). $L=5$ (solid), 10 (dashed), and 100 Å (dotted curve).

three-layer system, the situation is much more involved, so we present below only numerical results.

Now, consider the case where the screening is provided by the solute ions, while the solvent and the interlayer are supposed dispersionless. Another approximation used hereafter throughout the whole paper consists in the lack of self-consistency for all calculations. Specifically, the inverse Debye screening radius κ is considered constant up to the electrolyte solution border, whereas κ itself should be influenced by the image forces. A self-consistent approach was used, e.g., for the computation of the surface tension at the electrolyte solution/vacuum interface [83] (Onsager-Samaras problem [32]). The obtained series converged rapidly, and the overall correction was found to be small. The dependences $W_{\text{im}}(x)$ for $L=5$ Å and the neutral combination $\varepsilon_0^{\text{int}}=\varepsilon_0^{\text{solv}}=5$ are shown in Fig. 2 for certain bulk ion concentrations n_0. Such a situation simulates a conventional electrolytic cell [36,39] with the dense and the diffuse layers having the same background dielectric constant of the solvent, whereas ions do not penetrate into the dense layer.

All the curves do not diverge at the plane $x=0$, because the classical electrode is moved away and there is no short-wave dielectric mismatch between the solution and the interlayer. At the same time, the attraction moderated by the interlayer gives place to the repulsion due to the effective increase of the dielectric permittivity $\varepsilon_{el}(\mathbf{k})=\varepsilon_0^{\text{solv}}+\varepsilon_{\text{DH}}(\mathbf{k})$ induced by the ionic plasmalike contribution $\varepsilon_{\text{DH}}(\mathbf{k})$ [see Eq. (3)].

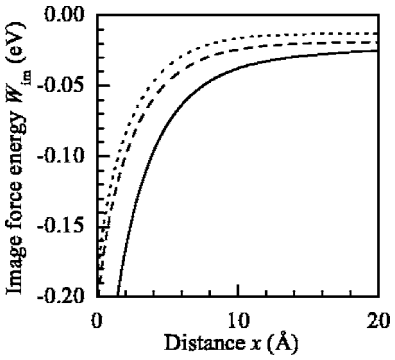

FIG. 15. The same as in Fig. 14 but for $n_0=0$. $L=5$ (solid), 10 (dashed), and 100 Å (dotted curve).

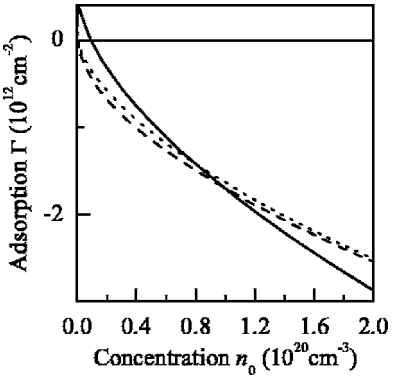

FIG. 16. The excess adsorption $\Gamma(n_0)$ calculated when the spatial dispersion of the dielectric permittivities of the solvent and interlayer is not taken ($\Lambda_{\text{int}}=\Lambda_{\text{solv}}=0$, solid curve) and taken [$\Lambda_{\text{int}}=\Lambda_{\text{solv}}=2$ (dashed) and 5 Å (dotted curve)] into account. $\varepsilon_0^{\text{int}}=\varepsilon_0^{\text{solv}}=5$, $L=5$ Å.

On the other hand, if $\varepsilon_0^{\text{int}}>\varepsilon_0^{\text{solv}}$ (the attractive combination), the ion contribution can not overcome the attraction both to the faraway metal and the adjacent interlayer in the near-layer region, as is demonstrated in Fig. 3. The image-force potential $W_{im}(x)$ diverges in this case as $-1/x$, so that the adsorption calculated by Eq. (14) becomes infinitely high.

In the opposite case, when $\varepsilon_0^{\text{int}}<\varepsilon_0^{\text{solv}}$ (the repulsive combination), the polarized metallic electrode is shielded in the neighborhood of even a thin interlayer, where $W_{\text{im}}(x)>0$, while the metal controls the behavior of the image forces in the bulk of the electrolyte solution, where $W_{\text{im}}(x)<0$. It is clearly seen from Fig. 4 for $n_0=0$. However, contrary to what is depicted in Fig. 3, a rise of the ion concentration n_0 gradually suppresses the negative branch of $W_{\text{im}}(x)$ shown in Fig. 4.

Provided such a complex spatial behavior of the image-force energy, it is difficult to predict *a priori* the relationship between the polarization-induced excess adsorption Γ, on the one hand, and the ion concentration n_0 or the screening parameters of the media involved, on the other hand. In fact, our specific calculations confirm the nontrivial character of the function $\Gamma(n_0)$. In Fig. 5, the curves $\Gamma(n_0)$ are demonstrated for a nominally electrostatically repulsive interlayer

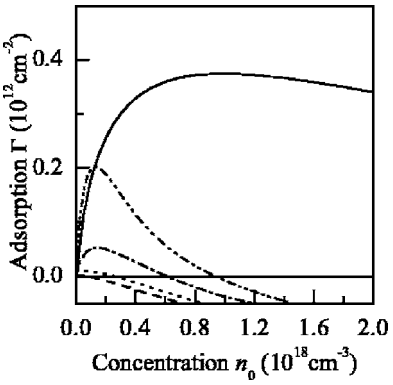

FIG. 17. A scaled-up section of Fig. 16 for small concentrations n_0.

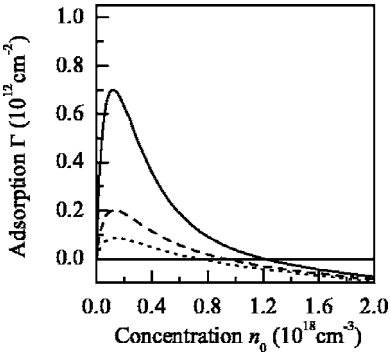

FIG. 18. The excess adsorption $\Gamma(n_0)$ calculated when the spatial dispersion of the dielectric permittivities of both the solvent and the interlayer is taken into account (the case $\varepsilon_0^{\mathrm{int}}=\varepsilon_0^{\mathrm{solv}}=5$) for various $\Lambda_{\mathrm{int}}=4.5$ (solid), 5 (dashed), and 5.5 Å (dotted curve). $\Lambda_{\mathrm{solv}}=5$ Å, $L=5$ Å.

with $\varepsilon_0^{\mathrm{int}} \leqslant \varepsilon_0^{\mathrm{solv}}$ and thickness $L=5$ Å. One can see that even for a substantial overshoot of $\varepsilon_0^{\mathrm{solv}}$ with respect to $\varepsilon_0^{\mathrm{int}}$, the adsorption remains positive for low enough n_0. The nonmonotonic form of $\Gamma(n_0)$, appropriate to the case $\varepsilon_0^{\mathrm{int}}=\varepsilon_0^{\mathrm{solv}} \equiv \varepsilon_0=5$ and depicted in Fig. 5 (solid curve), survives for other values of the common dielectric constant ε_0. This is readily seen from Fig. 6.

The attractive influence of the metal is severely weakened with increasing L. This trend can be inferred from the comparison of the dependences displayed in Figs. 6 and 7 calculated for the same values of $\varepsilon_0^{\mathrm{int}}=\varepsilon_0^{\mathrm{solv}}$. We see that for $L=10$ Å the amplitudes of the maxima of the curves $\Gamma(n_0)$ are an order of magnitude smaller than their counterparts for $L=5$ Å. Moreover, a transition to the negative values of $\Gamma(n_0)$ happens at lower n_0 if L increases.

C. Solvent and interlayer dielectric functions with spatial dispersion

The noticed tendency seems quite natural from general considerations, but one should bear in mind that the actual dielectric permittivities are by no means dielectric constants. Therefore, hereafter, we describe the permittivities by the interpolation formula (3). We should emphasize that in the sharp interface model, which is used in this work, the image-force potential in the nearest vicinity of the interface is de-

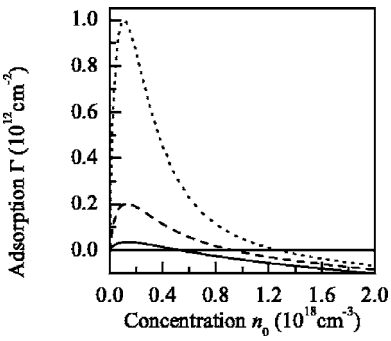

FIG. 19. The same as in Fig. 18 but for various $\Lambda_{\mathrm{solv}}=4.5$ (solid), 5 (dashed), and 5.5 Å (dotted curve). $\Lambda_{\mathrm{int}}=5$ Å.

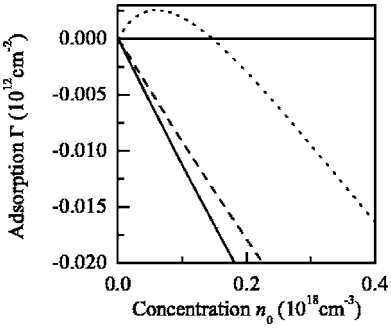

FIG. 20. The same as in Fig. 19 but for $\varepsilon_0^{\mathrm{int}}=3$ and $\varepsilon_0^{\mathrm{solv}}=10$ ($\varepsilon_0^{\mathrm{int}}<\varepsilon_0^{\mathrm{solv}}$). $L=10$ Å, $\Lambda_{\mathrm{int}}=5$ Å. $\Lambda_{\mathrm{solv}}=3$ (solid), 5 (dashed), and 7 Å (dotted curve).

termined just by the shortwave screening parameters $\varepsilon_*^{\mathrm{int}}$ and $\varepsilon_*^{\mathrm{solv}}$. In this region, they play the roles of effective dielectric constants and define whether the profile of the image force energy has a divergence or not. In this connection, we confine ourselves to the "asymptotically neutral case," i.e., the background (long-wave) constants $\varepsilon_0^{\mathrm{int}}$ and $\varepsilon_0^{\mathrm{solv}}$ will be varied, whereas both short-wavelength ones $\varepsilon_*^{\mathrm{int}}$ and $\varepsilon_*^{\mathrm{solv}}$ will be set equal to unity.

The dependences of the image force energy $W_{\mathrm{im}}(x)$ for the case $\varepsilon_0^{\mathrm{int}}>\varepsilon_0^{\mathrm{solv}}$ are depicted in Fig. 8. We remind the reader that in the constant permittivity approximation, ions, at an arbitrary $n_0 \neq 0$, are attracted by the interface in such a way that the excess adsorption becomes infinitely high (see Fig. 3). On the contrary, the integral in Eq. (13) converges at large q for any x, so that the overall attraction due to the dielectric mismatch is weakened in comparison to the dielectric constant case, and the Debye-Hückel screening contribution leads even to the repulsion at small distances. The curves shown in Fig. 8 were obtained for $\Lambda_{\mathrm{int}}=5<\Lambda_{\mathrm{solv}}=7$. If the opposite relationship takes place ($\Lambda_{\mathrm{int}}=5>\Lambda_{\mathrm{solv}}=3$), the ion screening may change the sign of the polarization force energy into the positive one within the whole relevant range of x, as is shown in Fig. 9. Note that for both previous figures, $\varepsilon_0^{\mathrm{int}}=10$, $\varepsilon_0^{\mathrm{solv}}=3$, and $L=10$ Å.

For the same solvent correlation lengths Λ_{int} and Λ_{solv} as in Fig. 9 but the repulsive combination of the background dielectric constants ($\varepsilon_0^{\mathrm{int}}=3$ and $\varepsilon_0^{\mathrm{solv}}=10$), the function $W_{\mathrm{im}}(x)$ changes its sign at $x \approx 32.5$ Å for the zero ion con-

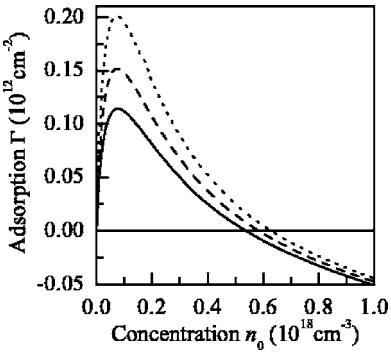

FIG. 21. The same as in Fig. 19 but for $\varepsilon_0^{\mathrm{int}}=10$ and $\varepsilon_0^{\mathrm{solv}}=3$ ($\varepsilon_0^{\mathrm{int}}>\varepsilon_0^{\mathrm{solv}}$). $L=10$ Å, $\Lambda_{\mathrm{int}}=5$ Å. $\Lambda_{\mathrm{solv}}=4.9$ (solid), 5 (dashed), and 5.1 Å (dotted curve).

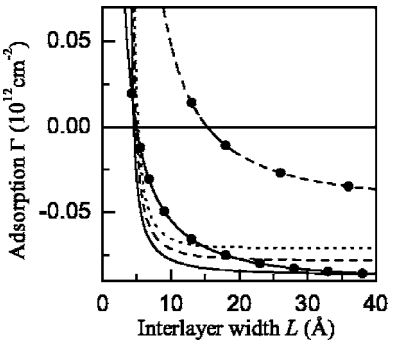

FIG. 22. The dependences $\Gamma(L)$ at $n_0=10^{18}$ cm^{-3}, $\varepsilon_0^{\mathrm{solv}}=5$, and for various $\varepsilon_0^{\mathrm{int}}=3$ (solid), 5 (dashed), and 8 (dotted curve). Curves with circles correspond to $\Lambda_{\mathrm{int}}=\Lambda_{\mathrm{solv}}=0$, and curves without circles to $\Lambda_{\mathrm{int}}=\Lambda_{\mathrm{solv}}=5$ Å.

centration n_0. It can be seen from Fig. 10. As n_0 increases, the polarization energy becomes completely repulsive. On the other hand, as stems from Fig. 11, the dependences $W_{\mathrm{im}}(x)$ have maxima at concentration-dependent distances x.

It is reasonable that the form of $W_{\mathrm{im}}(x)$ depends crucially on the separating interlayer thickness L. For instance, if $\Lambda_{\mathrm{int}}=\Lambda_{\mathrm{solv}}=5$ Å, $n_0=10^{18}$ cm^{-3}, $\varepsilon_0^{\mathrm{int}}=3$, and $\varepsilon_0^{\mathrm{solv}}=10$, all peculiarities of the repulsive curve $W_{\mathrm{im}}(x)$ observed at $L=5$ Å are wiped out at larger L (see Fig. 12). For $n_0=0$ and the same values of the other parameters, the curve $W_{\mathrm{im}}(x)$ changes its sign if $L=5$ Å but becomes entirely repulsive for larger L, as can be readily seen from Fig. 13.

The same trend of the rapid reduction of the metallic electrode influence by the increase of L can be inferred from Figs. 14 and 15 plotted for $\varepsilon_0^{\mathrm{int}}=10$ and $\varepsilon_0^{\mathrm{solv}}=3$.

The behavior of the image-force energy $W_{\mathrm{im}}(x)$ in the setup discussed markedly depends on several parameters. The number of those parameters is even larger than in the constant-dielectric case. That is why it is impossible to predict even the sign of the electrostatic adsorption Γ, to say nothing of its amplitude, *a priori*. Let us consider, e.g., the case of equal model parameters for the bulk of the electrolyte solution and the interlayer, the only difference being the dissolved ions absent from the interlayer (see Fig. 16). As stems from this figure, even in this simplest case, the approximations of the dielectric constants ($\Lambda_{\mathrm{int}}=\Lambda_{\mathrm{solv}}=0$) and dielectric functions lead to quite different results for $\Gamma(n_0)$. The same dependence is shown in Fig. 17 on a larger scale

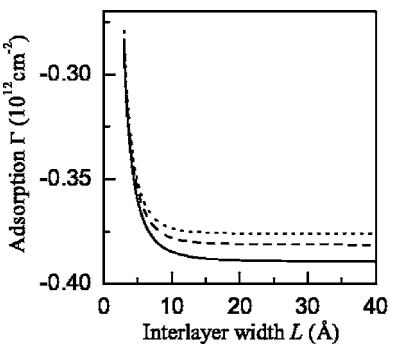

FIG. 23. The same as in Fig. 22 but for $n_0=10^{19}$ cm^{-3}.

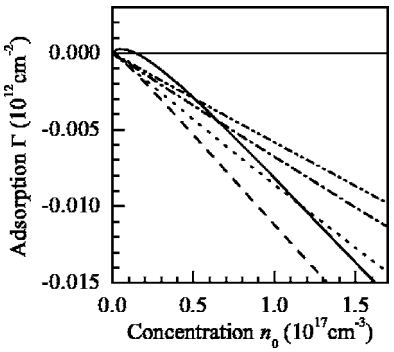

FIG. 24. The dependences $\Gamma(n_0)$ at the interface between a metal electrode covered with a dielectric layer and a 1:1 electrolyte solution for various background dielectric permittivities of the solvent $\varepsilon_0^{\mathrm{solv}}=3$ (solid), 5 (dashed), 25 (dotted), 50 (dotted-dashed), and 80 (dotted-dotted-dashed curve). $L=10$ Å, $\Lambda_{\mathrm{solv}}=3$ Å, $\varepsilon_0^{\mathrm{int}}=5$, and $\Lambda_{\mathrm{int}}=5$ Å.

for small n_0. One sees that all curves have maxima at some n_0 and the sign of Γ becomes negative for realistic values of $\Lambda_{\mathrm{int}}=\Lambda_{\mathrm{solv}}\leqslant 5$ Å and $n_0\gtrsim 10^{18}$ cm^{-3}. It means that the very existence of a thin solvent layer inaccessible to ions leads to the net electrostatic polarization-induced repulsion at the interface.

The whole picture is extremely sensitive to the values of Λ_{int} and Λ_{solv}, which by no means should coincide exactly. This is illustrated by Figs. 18 and 19.

If $\varepsilon_0^{\mathrm{int}}<\varepsilon_0^{\mathrm{solv}}$, the electrostatic adsorption Γ is not necessarily negative. The relationship between Λ_{int} and Λ_{solv} should also be made allowance for, as one can see from Fig. 20. Namely, for $\Lambda_{\mathrm{solv}}>\Lambda_{\mathrm{int}}$, the sign of Γ becomes ambiguous. Numerically, $\Gamma(n_0)$ is sensitive to the ratio $\Lambda_{\mathrm{int}}/\Lambda_{\mathrm{solv}}$ also in the case when $\varepsilon_0^{\mathrm{int}}>\varepsilon_0^{\mathrm{solv}}$ (see Fig. 21).

The dependences of Γ on the interlayer thickness L for two fixed ion concentrations n_0 are shown in Figs. 22 and 23. All the curves have the same character, the dependences being steep for small and saturating for large L. One can see that the dielectric-constant approximation fails in the quantitative description of $\Gamma(L)$. But the main conclusion is that for correctly simulated dielectric properties of the electrolyte solution (3), the attractive influence of the highly polarized metal is effectively screened by thick enough insulating interlayers, whatever the relationship between $\varepsilon_0^{\mathrm{int}}$ and $\varepsilon_0^{\mathrm{solv}}$.

So far we have dealt with solvents characterized by relatively small dielectric constants $\varepsilon_0^{\mathrm{solv}}$. At the same time, effective solvents usually possess much larger $\varepsilon_0^{\mathrm{solv}}$. For instance, $\varepsilon_0^{\mathrm{solv}}=78$ for water, and various alcohols possess $\varepsilon_0^{\mathrm{solv}}$ in the range 15–50 [91]. It turns out that all the trends reported above preserve also for much larger $\varepsilon_0^{\mathrm{solv}}$. Figure 24, where the dependences $\Gamma(n_0)$ are presented for different $3\leqslant\varepsilon_0^{\mathrm{solv}}\leqslant 80$ and the interlayer dielectric constant $\varepsilon_0^{\mathrm{int}}=5$, is an apt illustration of this statement.

IV. CONCLUSIONS

Using the electrostatic method with allowance for spatial dispersion of the dielectric permittivities [34,40,41], we have

carried out the investigation of image forces and the nonspecific ion Coulomb adsorption in electrolyte solutions near metal electrodes. The analysis has shown that the existence even of a very thin interlayer (with the thickness L comparable to an ion size) between a solution and an electrode can drastically reduce the polarization-induced ion attraction to the metal. Hence, the magnitude and even the sign of the extra adsorption Γ may change. In particular, if the dielectric constant of the interlayer $\varepsilon_0^{\mathrm{int}}$ is smaller than that of the solvent $\varepsilon_0^{\mathrm{solv}}$, the attraction transforms into a repulsion, especially for large ion concentrations n_0. Our calculations have demonstrated that the proper account of the spatial dispersion for both dielectric permittivities $\varepsilon^{\mathrm{int}}(\mathbf{k})$ and $\varepsilon^{\mathrm{solv}}(\mathbf{k})$ is necessary to obtain a correct result, whereas the constant approximation for $\varepsilon^{\mathrm{int}}(\mathbf{k})$ and $\varepsilon^{\mathrm{solv}}(\mathbf{k})$ is a very crude one.

Strictly speaking, the near-electrode layer with the dielectric (screening) properties different from those in the bulk of the solution always exists, e.g., as the dense inner layer of the Gouy-Chapman theory [2,36,37,39]. Our calculations with $L \leqslant 5$ Å simulated this situation. The opposite case of the artificially deposited on the electrode interlayer of an arbitrary thickness is more interesting because this interlayer may serve as a powerful tool to control the physical adsorption in the electrochemical cells. At large n_0, the excess Coulomb nonspecific adsorption Γ may constitute an appreciable part of the total adsorption.

The developed theory for the image-force energy W_{im} can be applied to any three-layer system with solid or liquid constituents and makes it possible to estimate the validity of the simple dielectric-constant approximation often used in literature. As for the results concerning $\Gamma(n_0)$, they describe electrochemical cells, where the role of the inner layer is essential or the electrode is covered by an additional dielectric layer.

LCDs can be considered as the most important objects to be analyzed on the basis of the elaborated concept because many of their properties are influenced by electrodynamic processes taking place in the electrode neighborhood. Particularly, in LC cells spontaneous and electrically induced ion adsorption results in the strong increase of the driving voltage for various electro-optical LCDs [59]. The adsorbed ions form the charged shield, responsible for the residual image of the previous frame, which often survives on a liquid crystal display (the so-called sticking effect) [92,93]. This phenomenon may strongly impair the quality of LCDs and needs to be diminished. At the same time, light-induced changes of the adsorbed current-carrier concentration in the electrolyte-plasma double layer near the interface govern the recording of photorefractive gratings in LCs and allow the development of optically controlled switchers [94].

In the case when there are additional polymer layers on various dielectric or metallic substrates, the influence of the dissolved ions on anchoring of LC molecules was studied by several groups [61,64,66,95–108]. However, the causes of the ion adsorption considered in those papers did not include the dielectric mismatch between the adjacent constituting layers and, as a consequence, did not make allowance for the image forces. To our knowledge, there are only two papers where the latter were referred to.

In the first one [64], the adsorption energy of the positive ions was identified with the classical image-force energy truncated at the distance equal to the radius of the adsorbed positive ion. This may be regarded as an estimation only. Moreover, the very concept of the selective adsorption in Ref. [64], totally neglecting the negative ion contribution to Γ, differs from our purely electrostatic approach, where positive and negative charges are treated on equal footing and their contributions to Γ have the same values for symmetrical electrolytes. In the second work of the same group [61], a decrease of the anchoring strength under the influence of the ultraviolet illumination was interpreted in terms of classical image forces between dipoles, the latter differing for *trans*- and *cis*-isomers.

Since the calculations presented above clearly show the sensitivity of the electrostatic adsorption Γ to the account of the spatial dispersion for the relevant dielectric functions, we think that properly treated image forces in two- or three-layer geometry should always be taken into account for charged particle adsorption in LC and organic liquid electrochemical cells. Nevertheless, amazingly, the dielectric mismatch at the boundaries have been out of consideration so far while treating many problems in LCDs *even in the classical approximation*. At the same time, a typical LC cell consists of a glass substrate covered with a highly conductive electrode, which in turn is covered with a thin polymer layer, and just the mismatch between dielectric functions for these three media crucially governs the distribution of ions near the polymer surface. This paper may be considered as a step in the outlined direction.

ACKNOWLEDGMENTS

A.M.G. and A.I.V. are grateful to Kasa im. Jósefa Mianowskiego and Fundacja na Rzecz Nauki Polskiej for the financial support of their visits to Warsaw.

[1] A. G. Volkov, D. W. Deamer, D. L. Tanelian, and V. S. Markin, Prog. Surf. Sci. **53**, 1 (1996).
[2] S. L. Carnie and G. M. Torrie, Adv. Chem. Phys. **56**, 141 (1984).
[3] J. R. Manson and R. H. Ritchie, Phys. Rev. B **24**, 4867 (1981).
[4] A. G. Eguiluz, Phys. Rev. B **23**, 1542 (1981).
[5] A. A. Kornyshev, A. I. Rubinshtein, and M. A. Vorotyntsev, Phys. Status Solidi B **84**, 125 (1977).
[6] A. M. Gabovich, L. G. Il'chenko, E. A. Pashitskii, and Yu. A. Romanov, Zh. Eksp. Teor. Fiz. **75**, 249 (1978).
[7] K. Holub and A. A. Kornyshev, J. Chem. Soc., Faraday Trans. 2 **76**, 67 (1980).
[8] A. A. Kornyshev, Electrochim. Acta **26**, 1 (1981).
[9] A. A. Kornyshev, M. A. Vorotyntsev, H. Nielsen, and

J. Ulstrup, J. Chem. Soc., Faraday Trans. 2 **78**, 217 (1982).
[10] A. A. Kornyshev, J. Chem. Soc., Faraday Trans. 2 **79**, 651 (1983).
[11] A. A. Kornyshev and G. Sutmann, J. Chem. Phys. **104**, 1524 (1996).
[12] P. A. Bopp, A. A. Kornyshev, and G. Sutmann, Phys. Rev. Lett. **76**, 1280 (1996).
[13] A. A. Kornyshev and G. Sutmann, Phys. Rev. Lett. **79**, 3435 (1997).
[14] A. A. Kornyshev, S. Leikin, and G. Sutmann, Electrochim. Acta **42**, 849 (1997).
[15] A. A. Kornyshev and G. Sutmann, J. Electroanal. Chem. **450**, 143 (1998).
[16] P. A. Bopp, A. A. Kornyshev, and G. Sutmann, J. Chem. Phys. **109**, 1939 (1998).
[17] A. A. Kornyshev and G. Sutmann, J. Mol. Liq. **82**, 151 (1999).
[18] D. A. Cherepanov, Phys. Rev. Lett. **93**, 266104 (2004).
[19] A. A. Kornyshev and M. A. Vorotyntsev, Can. J. Chem. **59**, 2031 (1981).
[20] A. M. Gabovich and A. I. Voitenko, Electrochim. Acta **31**, 777 (1986).
[21] M. L. Belaya, V. G. Levadny, and M. V. Feigelman, Zh. Eksp. Teor. Fiz. **91**, 1336 (1986).
[22] P. Attard, D. Wei, and G. N. Patey, Chem. Phys. Lett. **172**, 69 (1990).
[23] B. B. Smith and C. A. Koval, J. Electroanal. Chem. Interfacial Electrochem. **277**, 43 (1990).
[24] S. Leikin and A. A. Kornyshev, J. Chem. Phys. **92**, 6890 (1990).
[25] M. A. Vorotyntsev and P. V. Mityushev, Electrochim. Acta **36**, 401 (1991).
[26] J. C. Inkson, J. Phys. C **4**, 591 (1971).
[27] A. I. Voitenko and A. M. Gabovich, Elektrokhimiya **18**, 612 (1982).
[28] A. M. Gabovich and A. I. Voitenko, Electrochim. Acta **28**, 1771 (1983).
[29] A. I. Voitenko and A. M. Gabovich, Elektrokhimiya **22**, 1220 (1986).
[30] A. I. Voitenko and A. M. Gabovich, Elektrokhimiya **25**, 48 (1989).
[31] A. M. Gabovich and A. I. Voitenko, Electrochim. Acta **35**, 545 (1990).
[32] L. Onsager and N. N. T. Samaras, J. Chem. Phys. **2**, 528 (1934).
[33] D. E. Beck and V. Celli, Phys. Rev. B **2**, 2955 (1970).
[34] A. M. Gabovich, L. G. Il'chenko, E. A. Pashitskii, and Yu. A. Romanov, Surf. Sci. **94**, 179 (1980).
[35] F. Bechstedt, R. Enderlein, and D. Reichardt, Phys. Status Solidi B **117**, 261 (1983).
[36] W. Schmickler and D. Henderson, Prog. Surf. Sci. **22**, 323 (1986).
[37] M. A. Vorotyntsev and A. A. Kornyshev, Electrochim. Acta **20**, 3 (1984).
[38] J. Heinrichs, Phys. Rev. B **8**, 1346 (1973).
[39] B. B. Damaskin and O. A. Petrii, *Introduction to Electrochemical Kinetics* (Vysshaya Shkola, Moscow, 1983), in Russian.
[40] L. G. Il'chenko, E. A. Pashitskii, and Yu. A. Romanov, Surf. Sci. **121**, 375 (1982).
[41] A. M. Gabovich, V. M. Rozenbaum, and A. I. Voitenko, Surf. Sci. **186**, 523 (1987).
[42] A. M. Gabovich and V. M. Rozenbaum, Fiz. Tekh. Poluprovodn. (S.-Peterburg) **18**, 498 (1984).
[43] E. P. Pokatilov, V. M. Fomin, and S. I. Beril, *Oscillatory Excitations, Polarons and Excitons in Multilayer Systems and Superlattices* (Shtiintsa, Kishinev, 1990), in Russian.
[44] F. T. Vas'ko, *Electron States and Optical Transitions in Semiconductor Heterostructures* (Naukova Dumka, Kiev, 1993), in Russian.
[45] D. J. Paul, Semicond. Sci. Technol. **19**, R75 (2004).
[46] V. N. Ojha, P. K. Bhatnagar, S. R. Dhariwal, and K. K. Sharma, J. Appl. Phys. **53**, 1734 (1982).
[47] A. Tugulea and D. Dascălu, J. Appl. Phys. **56**, 2823 (1984).
[48] A. G. O'Neill, J. Appl. Phys. **58**, 4740 (1985).
[49] V. K. Khanna, Phys. Rep. **398**, 67 (2004).
[50] R. Kjellander, J. Chem. Soc., Faraday Trans. 2 **80**, 1323 (1984).
[51] A. A. Kornyshev, J. Electroanal. Chem. Interfacial Electrochem. **204**, 79 (1986).
[52] M. L. Belaya, M. V. Feigelman, and V. G. Levadny, Chem. Phys. Lett. **126**, 361 (1986).
[53] S. Leikin, J. Chem. Phys. **95**, 5224 (1991).
[54] D. Y. C. Chan and D. A. McQuarrie, J. Phys. (Paris), Colloq. **88**, 1433 (1992).
[55] J. P. Cleveland, T. E. Schäffer, and P. K. Hansma, Phys. Rev. B **52**, R8692 (1995).
[56] J. Israelachvili and H. Wennerström, Nature **379**, 219 (1996).
[57] L. I. Boguslavsky, *Bioelectrochemical Phenomena and the Interface* (Nauka, Moscow, 1978), in Russian.
[58] R. R. Netz, Eur. Phys. J. E **3**, 131 (2000).
[59] L. M. Blinov and V. G. Chigriniv, *Electrooptic Effects in Liquid Crystal Materials* (Springer-Verlag, New York, 1994).
[60] A. L. Alexe-Ionescu, A. Th. Ionescu, N. Scaramuzza, G. Strangi, C. Versace, G. Barbero, and R. Bartolino, Phys. Rev. E **64**, 011708 (2001).
[61] G. Barbero, D. Olivero, N. Scaramuzza, G. Strangi, and C. Versace, Phys. Rev. E **69**, 021713 (2004).
[62] A. M. Brodsky and M. I. Urbakh, *Electrodynamics of Metal/Electrolyte Interface* (Nauka, Moscow, 1989), in Russian.
[63] F. Bechstedt and M. Scheffler, Surf. Sci. Rep. **18**, 145 (1993).
[64] G. Barbero, A. K. Zvezdin, and L. R. Evangelista, Phys. Rev. E **59**, 1846 (1999).
[65] J. F. Joanny, Eur. Phys. J. B **9**, 117 (1999).
[66] V. G. Nazarenko, V. M. Pergamenshchik, O. V. Koval'chuk, A. B. Nych, and B. I. Lev, Phys. Rev. E **60**, 5580 (1999).
[67] G. Barbero and D. Olivero, Phys. Rev. E **65**, 031701 (2002).
[68] A. Shafir and D. Andelman, Phys. Rev. E **70**, 061804 (2004).
[69] C. Friedsam, H. E. Gaub, and R. R. Netz, Europhys. Lett. **72**, 844 (2005).
[70] A. K. Shchekin and V. V. Borisov, Kolloidn. Zh. **67**, 850 (2005).
[71] K.-R. Schulze and K. Unger, Phys. Status Solidi B **66**, 491 (1974).
[72] J. Lindhard, K. Dan. Vidensk. Selsk. Mat. Fys. Medd. **28**, 1 (1954).
[73] W. A. Harrison, *Solid State Theory* (McGraw-Hill, New York, 1970).
[74] A. M. Gabovich and A. I. Voitenko, Phys. Status Solidi B **110**, 407 (1982).
[75] A. M. Gabovich, L. G. Il'chenko, and E. A. Pashitskii, Surf. Sci. **130**, 373 (1983).

[76] C. Kittel, *Introduction to Solid State Physics* (John Wiley and Sons, New York, 1995).
[77] K. S. Singwi and M. P. Tosi, Solid State Phys. **36**, 177 (1981).
[78] O. V. Dolgov, D. A. Kirzhnits, and E. G. Maksimov, Rev. Mod. Phys. **53**, 81 (1981).
[79] O. V. Dolgov, D. A. Kirzhnits, and E. G. Maksimov, in *Superconductivity, Superdiamagnetism, Superfluidity*, edited by V. L. Ginzburg (Mir, Moscow, 1987), p. 18–68.
[80] L. Cheng, P. Fenter, K. L. Nagy, M. L. Schlegel, and N. C. Sturchio, Phys. Rev. Lett. **87**, 156103 (2001).
[81] Yu. A. Romanov, Zh. Eksp. Teor. Fiz. **47**, 2119 (1964).
[82] H. S. Harned and B. B. Owen, *The Physical Chemistry of Electrolytic Solutions* (Reinhold, New York, 1950).
[83] T. Nakamura, T. Tanaka, and Y. Izumitani, J. Phys. Soc. Jpn. **51**, 2271 (1982).
[84] D. S. Dean and R. R. Horgan, Phys. Rev. E **69**, 061603 (2004).
[85] T. S. Rahman and A. A. Maradudin, Phys. Rev. B **21**, 504 (1980).
[86] L. I. Daikhin, A. A. Kornyshev, and M. Urbakh, J. Chem. Phys. **108**, 1715 (1998).
[87] R. G. Barrera, O. Guzmán, and B. Balaguer, Am. J. Phys. **46**, 1172 (1978).
[88] E. P. Pokatilov, S. I. Beril, N. N. Semenovskaya, and M. Fahood, Phys. Status Solidi B **158**, 165 (1990).
[89] N. D. Lang, Solid State Phys. **28**, 225 (1973).
[90] M. B. Partensky, Usp. Fiz. Nauk **128**, 69 (1979).
[91] Ch. Mann, in *Electroanalytical Chemistry*, vol. 3, edited by A. J. Bard (Marcel Dekker, New York, 1969), p. 57–134.
[92] A. Lien, C.-J. Chen, H. Inoue, and Y. Saitoh, SID Int. Symp. Digest Tech. Papers 203 (1997).
[93] I. Gerus, A. Glushchenko, Yu. Kurioz, Yu. Reznikov, and O. Tereshchenko, Opto-Electron. Rev. **12**, 281 (2004).
[94] J. Merlin, E. Chao, M. Winkler, K. D. Singer, P. Korneychuk, and Y. Reznikov, Opt. Express **13**, 5024 (2005).
[95] A. L. Alexe-Ionescu, G. Barbero, and A. G. Petrov, Phys. Rev. E **48**, R1631 (1993).
[96] V. G. Nazarenko and O. D. Lavrentovich, Phys. Rev. E **49**, R990 (1994).
[97] G. Barbero, L. R. Evangelista, and N. V. Madhusudana, Eur. Phys. J. B **1**, 327 (1998).
[98] V. S. U. Fazio and L. Komitov, IEEE Electron Device Lett. **46**, 38 (1999).
[99] R. Meister and B. Jérôme, J. Appl. Phys. **86**, 2473 (1999).
[100] U. Kühnau, A. G. Petrov, G. Klose, and H. Schmiedel, Phys. Rev. E **59**, 578 (1999).
[101] S. Ponti, P. Ziherl, C. Ferrero, and S. Žumer, Liq. Cryst. **26**, 1171 (1999).
[102] H. A. Pereira and L. R. Evangelista, Eur. Phys. J. E **3**, 123 (2000).
[103] L. R. Evangelista and G. Barbero, Phys. Rev. E **64**, 021101 (2001).
[104] V. S. U. Fazio, F. Nannelli, and L. Komitov, Phys. Rev. E **63**, 061712 (2001).
[105] D. Olivero, L. R. Evangelista, and G. Barbero, Phys. Rev. E **65**, 031721 (2002).
[106] G. Barbero, L. R. Evangelista, and L. Komitov, Phys. Rev. E **65**, 041719 (2002).
[107] M. Scalerandi, P. Pagliusi, G. Cipparrone, and G. Barbero, Phys. Rev. E **69**, 051708 (2004).
[108] G. Barbero, Phys. Rev. E **71**, 062201 (2005).